Liquid Crystals
Publication details, including instructions for authors and subscription information:
http://www.informaworld.com/smpp/title~content=t713926090

Ferrielectric and antiferroelectric chiral twin liquid crystals showing a stable chiral nematic phase

Isa Nishiyama; Jun Yamamoto; John W. Goodby; Hiroshi Yokoyama

Online publication date: 11 November 2010

To cite this Article Nishiyama, Isa , Yamamoto, Jun , Goodby, John W. and Yokoyama, Hiroshi(2002) 'Ferrielectric and antiferroelectric chiral twin liquid crystals showing a stable chiral nematic phase', Liquid Crystals, 29: 11, 1409 — 1423
To link to this Article: DOI: 10.1080/0267829021000030668
URL: http://dx.doi.org/10.1080/0267829021000030668

LIQUID CRYSTALS, 2002, VOL. 29, NO. 11, 1409–1423

Taylor & Francis
Taylor & Francis Group

Ferrielectric and antiferroelectric chiral twin liquid crystals showing a stable chiral nematic phase

ISA NISHIYAMA*, JUN YAMAMOTO, JOHN W. GOODBY† and HIROSHI YOKOYAMA

Yokoyama Nano-structured Liquid Crystal Project, JST, TRC 5-9-9 Tokodai, Tsukuba 300-2635, Japan

†Department of Chemistry, The University of Hull, Hull HU6 7RX, UK

(*Received 30 April 2002; accepted 22 July 2002*)

A homologous series of chiral twin liquid crystals possessing identical chiral moieties at both peripheral ends, i.e. optically active α,ω-bis{4-[(4′-(1-methylheptyloxycarbonyl)-4-biphenylyl)-oxycarbonyl]phenoxy}alkanes, has been prepared and their liquid crystalline properties investigated. The homologues preferred to show the ferrielectric and/or antiferroelectric phase rather than the ferroelectric phase. With ascending central spacer length, the temperature range of the ferrielectric phase became narrow and eventually disappeared for the dodecyl homologue, suggesting that the coupling in motion and/or direction between two mesogenic parts of each twin molecule has an important effect on the stabilization of the ferrielectric phase. The octyl and dodecyl homologues showed a wide temperature range chiral nematic phase (ca. 10°C or more), so that these compounds were found to be the first examples showing antiferroelectric and/or ferrielectric phases with a broad temperature range of the chiral nematic phase. X-ray diffraction studies showed that the homologues tend to form a mono-layered structure. The formation of a relatively well defined layered structure was also indicated, which is considered to be important for generating anticlinic ordering in the antiferroelectric and ferrielectric phases. An isotropic–isotropic transition characterized by the emergence of a broad diffuse DSC peak was observed for the even-membered homologues.

1. Introduction

So far, a variety of antiferroelectric and ferrielectric liquid crystals, as well as ferroelectric materials, has been prepared and their properties investigated from both the practical and scientific points of view [1]. The major difference in the molecular assembly between these phases lies in the tilt direction from one smectic layer to another. The ferroelectric phase shows synclinic molecular ordering, whereas the antiferroelectric or ferrielectric character is generated by the existence of an anticlinic molecular assembly. Another important difference has also been noticed; that is, ferroelectric materials possessing a chiral nematic phase can easily be obtained, but antiferroelectric and ferrielectric characteristics normally appear in the absence of the chiral nematic phase. The existence of the nematic phase above the smectic phase is considered to produce a better alignment of the molecules in the smectic phase and this is important for the applications of display and switching devices [2]. Possession of the nematic phase alone is not a perfect solution for achieving a high quality alignment in the smectic phase and therefore a new type of switching mode using antiferroelectric materials with a 45° tilt has recently been proposed as a novel answer to overcoming the difficulty of obtaining good alignment for antiferroelectric materials [3]. Nevertheless, it is still important to investigate the reason why antiferroelectric and ferrielectric materials have a tendency not to show the chiral nematic phase, so that a better understanding of the origin of the antiferroelectricity and ferrielectricity can be achieved.

Only a few compounds have so far been reported to show the chiral nematic phase and also antiferroelectric or related characteristics. Aoki and Nohira reported that the racemic modification of TFMB, figure 1 (*a*), shows the anticlinic phase with the presence of a narrow temperature range (*c*. 1°C) of nematic phase [4]. Since the pure enantiomers themselves have been reported not to show the chiral nematic phase, but to show the twist grain boundary (TGB) phase, it is not clear whether the antiferroelectric phase with the presence of the chiral nematic phase can be obtained by adjusting the optical purity. Yoshizawa *et al.* reported that a non-symmetric achiral twin compound consisting of cyanobiphenyl and phenylpyrimidine moieties, 8PY11OCB figure 1 (*b*), shows the anticlinic phase and the nematic phase [5]; however, the induction of antiferroelectricity, for example

*Author for correspondence; e-mail: isanishi@nanolc.jst.go.jp

Liquid Crystals ISSN 0267-8292 print/ISSN 1366-5855 online © 2002 Taylor & Francis Ltd
http://www.tandf.co.uk/journals
DOI: 10.1080/0267829021000030668

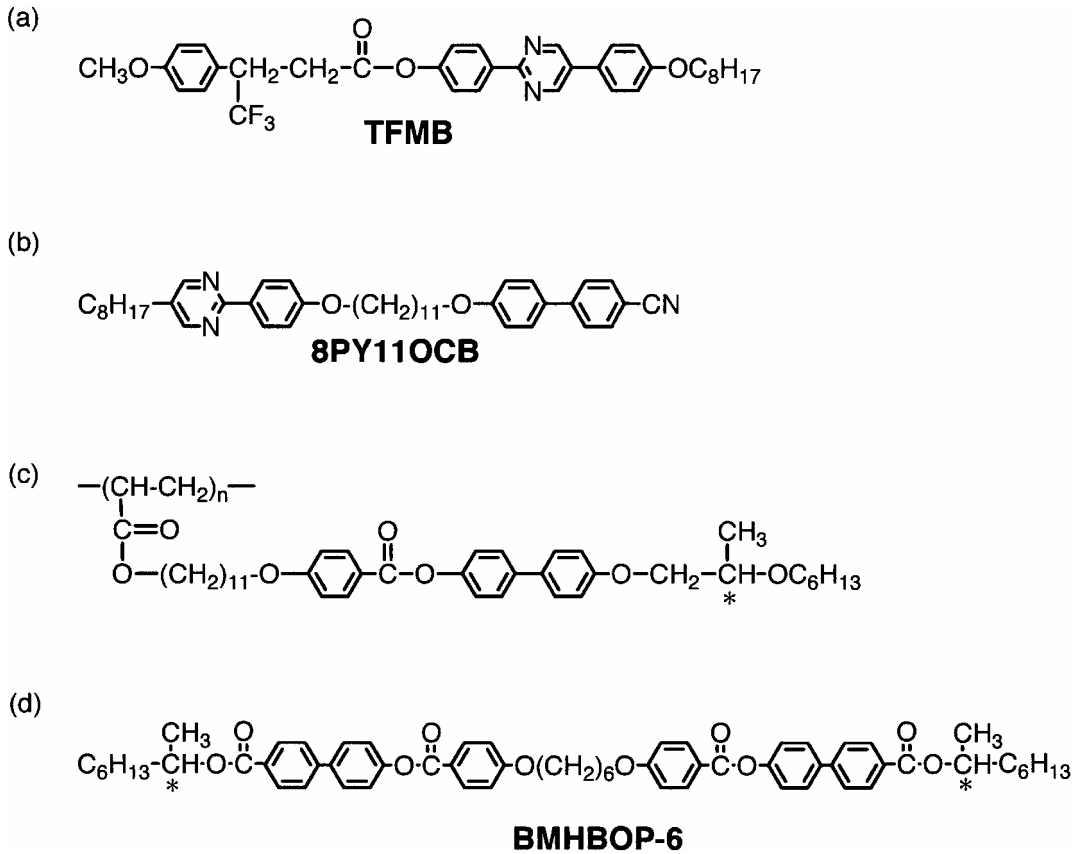

Figure 1. Molecular structures of the compounds so far reported to show the chiral nematic phase and the antiferroelectric phase and related characteristics.

by introducing chirality in the system, has not yet been reported. Another interesting phase transition behaviour has been reported for a chiral side group liquid crystal polymer [6], figure 1 (*c*), where the polymer shows the chiral nematic phase as well as smectic phases possessing characteristic layer stacking structures where the molecules assemble in a similar way to that in the antiferroelectric or ferrielectric phase. More recently, a 1 : 1 mixture of (*S*,*S*)- and (*R*,*R*)-isomers of a symmetric chiral twin compound possessing identical chiral moieties at both peripheral ends of the molecular structure, BMHBOP-6 figure 1 (*d*), has been reported to show the nematic phase; whereas the (*S*,*S*)- and (*R*,*R*)-isomers themselves did not show the chiral nematic phase [7]. Furthermore, the induction of the chiral nematic phase has also been observed in some mixtures between optically active BMHBOP-6 and the analogous monomer, even though the twin and monomeric compounds themselves do not exhibit the chiral nematic phase [8].

These results indicate that the symmetric chiral twin system may be a good candidate for obtaining antiferroelectric and ferrielectric materials showing the chiral nematic phase. Thus, in this study, a homologous series of optically active α,ω-bis{4-[(4′-(1-methylheptyloxycarbonyl)-4-biphenylyl)oxycarbonyl]phenoxy}-alkanes (BMHBOP-*n*) was prepared and the liquid crystalline properties investigated. The octyl homologue (BMHBOP-8) and the dodecyl homologue (BMHBOP-12) were found to be the first antiferroelectric/ferrielectric and antiferroelectric materials respectively, showing a broad temperature range of the chiral nematic phase.

2. Experimental

2.1. *Preparation of compounds*

The chiral twin homologues BMHBOP-*n* were prepared according to the procedure reported for BMHBOP-6 [7] (see the scheme). The final twin compounds were

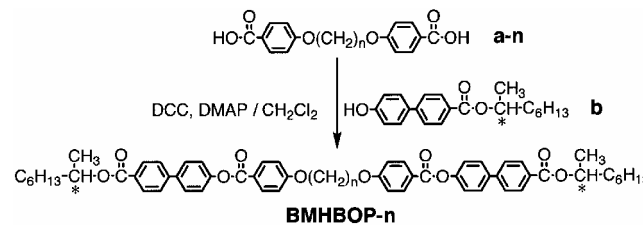

Scheme. Preparation of BMHBOP-*n*.

obtained by esterification between the respective α,ω-bis-(4-carboxyphenoxy) alkanes (**a**–**n**) and optically active (*S*)- or (*R*)-1-methylheptyl 4-hydroxybiphenyl-4′-carboxylate (**b**) in the presence of dicyclohexylcarbodiimide (DCC) and *N*,*N*-dimethylaminopyridine (DMAP) [9]. The α,ω-bis-(4-carboxyphenoxy) alkanes (**a**–**n**) were prepared according to reported preparation procedures [10]. Standard synthetic methods were also used for obtaining the optically active 1-methylheptyl 4-hydroxybiphenyl-4′-carboxylates (**b**) [11, 12], where (*S*)-2-octanol (Azmax. Co. Ltd., 99%ee) or (*R*)-2-octanol (Azmax. Co. Ltd., 99%ee) was used as the starting chiral alcohol without further purification.

The purification of the final products was carried out using column chromatography over silica gel (70–230 mesh) (Sigma-Aldrich Co.) using a dichrolomethane/hexane mixture as the eluent, followed by recrystallization from an ethanol/ethyl acetate mixture. The structures of the materials were elucidated by a variety of spectral methods. Infrared (IR) spectroscopy was carried out using a Shimadzu FTIR-8100A infrared spectrophotometer, proton nuclear magnetic resonance (^{1}H NMR) spectrometry was carried out using a Brucker DRX500 (^{1}H NMR, 500 MHz) nuclear magnetic resonance spectrometer, and mass spectrometry (MS) was carried out using a JEOL, JMS-700, using an FD/MS method. The analyses of the structures of the products and intermediates by spectroscopic methods were found to be consistent with the predicted structures. The purities of all of the final compounds were checked by reverse-phase and normal-phase high-performance liquid chromatography (HPLC). Reverse-phase HPLC was carried out using a ZORBAX, Eclipse XDB-C8 column. A mixture of acetonitrile/THF (93/7) was used as eluent. Detection of products was achieved by UV irradiation ($\lambda = 280$ nm). Similarly, normal-phase HPLC was carried out using a Shimadzu CLC-SIL(M) column. Dichloromethane was used as eluent. Detection of products was achieved by UV irradiation ($\lambda = 254$ nm).

2.1.1. *(S,S)-α,ω-Bis{4-[(4′-(1-methylheptyloxycarbonyl)-4-biphenylyl)oxycarbonyl]phenoxy}heptane, (S,S)-BMHBOP-7*

α,ω-Bis-(4-carboxyphenoxy) heptane (**a**–**7**) (0.74 g, 2.0 mmol), (*S*)-1-methylheptyl 4-hydroxybiphenyl-4′-carboxylate ((*S*)-**b**) (1.30 g, 4.0 mmol) and DMAP (0.05 g, 0.4 mmol) were added to dry dichloromethane (10 ml). DCC (1.23 g, 6.0 mmol) was then added and the resulting mixture stirred at room temperature for one day. Precipitated materials were removed by filtration. After removal of the solvent by evaporation under reduced pressure, the residue was purified by column chromatography using a dichrolomethane/hexane (10/3) mixture as the eluent, and recrystallized from an ethanol/ethyl acetate (1/1) mixture, giving a colourless solid product; yield 0.88 g, (41%). δH (500 MHz, $CDCl_3$, TMS): 8.17 (m, 4H, Ar-**H**), 8.11 (m, 4H, Ar-**H**), 7.65 (m, 8H, Ar-**H**), 7.31 (m, 4H, Ar-**H**), 6.98 (m, 4H, Ar-**H**), 5.18 (m, 2H, $-C^*\mathbf{H}(CH_3)-$), 4.07 (t, 4H, $-C\mathbf{H}_2O-$, $^3J = 6.5$ Hz), 1.86 (m, 4H, $-C\mathbf{H}_2CH_2O-$), 1.75–1.30 (m, 32H, aliphatic-**H**), 0.88 (t, 6H, $-C\mathbf{H}_3$, $^3J = 6.9$ Hz). ν/cm^{-1} (KBr); 2942, 2859 (C–H str.), 1746, 1717 (C=O str.), 1605 (C–C str.), 843 (1,4-disub. C–H out-of-plane deformation (o.o.p.d)). m/z: 988 (M^+), 663, 494, 325. HPLC purity: normal phase SIL(M) column 99.9%; reverse phase C8 column 98.8%.

2.1.2. *(S,S)-α,ω-Bis{4-[(4′-(1-methylheptyloxycarbonyl)-4-biphenylyl)oxycarbonyl]phenoxy}octane, (S,S)-BMHBOP-8*

α,ω-Bis-(4-carboxyphenoxy) octane (**a**–**8**) (0.77 g, 2.0 mmol) and (*S*)-1-methylheptyl 4-hydroxybiphenyl-4′-carboxylate ((*S*)-**b**) (1.30 g, 4.0 mmol) were esterified using DMAP (0.05 g, 0.4 mmol), dry dichloromethane (10 ml) and DCC (1.23 g, 6.0 mmol) as described for BMHBOP-7. After removal of the solvent, the residue was purified by column chromatography using a dichrolomethane/hexane (20/3) mixture as eluent, and recrystallized from an ethanol/ethyl acetate (1/4) mixture, giving a colourless solid product; yield 0.95 g, (48%). δH (500 MHz, $CDCl_3$, TMS): 8.17 (m, 4H, Ar-**H**), 8.11 (m, 4H, Ar-**H**), 7.65 (m, 8H, Ar-**H**), 7.31 (m, 4H, Ar-**H**), 6.98 (m, 4H, Ar-**H**), 5.18 (m, 2H, $-C^*\mathbf{H}(CH_3)-$), 4.07 (t, 4H, $-C\mathbf{H}_2O-$, $^3J = 6.5$ Hz), 1.84 (m, 4H, $-C\mathbf{H}_2CH_2O-$), 1.75–1.30 (m, 34H, aliphatic-**H**), 0.88 (t, 6H, $-C\mathbf{H}_3$, $^3J = 6.9$ Hz). ν/cm^{-1} (KBr): 2934, 2857 (C–H str.), 1740, 1713 (C=O str.), 1607 (C–C str.), 847 (1,4-disub. C–H o.o.p.d). m/z: 1002 (M^+), 677, 501, 325. HPLC purity: normal phase SIL(M) column 100%; reverse phase C8 column 99.3%.

2.1.3. *(R,R)-α,ω-Bis{4-[(4′-(1-methylheptyloxycarbonyl)-4-biphenylyl)oxycarbonyl]phenoxy}octane, (R,R)-BMHBOP-8*

α,ω-Bis-(4-carboxyphenoxy) octane (**a**–**8**) (0.77 g, 2.0 mmol) and (*R*)-1-methylheptyl 4-hydroxybiphenyl-4′-carboxylate ((*R*)-**b**) (1.30 g, 4.0 mmol) were esterified using DMAP (0.05 g, 0.4 mmol), dry dichloromethane (10 ml) and DCC (1.23 g, 6.0 mmol) as described for BMHBOP-7. After removal of the solvent, the residue was purified by column chromatography using a dichrolomethane/hexane (5/1–5/2) mixture as eluent, and recrystallized from an ethanol/ethyl acetate (1/4) mixture, giving a colourless solid product; yield = 1.02 g, (51%). δH (500 MHz, $CDCl^3$, TMS): 8.17 (m, 4H, Ar-**H**), 8.11 (m, 4H, Ar-**H**), 7.65 (m, 8H, Ar-**H**), 7.31 (m, 4H, Ar-**H**), 6.98 (m, 4H, Ar-**H**), 5.18 (m, 2H, $-C^*\mathbf{H}(CH_3)-$), 4.07 (t, 4H, $-C\mathbf{H}_2O-$, $^3J = 6.5$ Hz), 1.84

(m, 4H, $^{-}C\mathbf{H}_2CH_2O^{-}$), 1.75–1.30 (m, 34H, aliphatic-**H**), 0.88 (t, 6H, $^{-}C\mathbf{H}_3$, $^3J = 6.9$ Hz). ν/cm^{-1} (KBr): 2934, 2857 (C–H str.), 1740, 1713 (C=O str.), 1607 (C–C str.), 847 (1,4-disub. C–H o.o.p.d). m/z: 1002 (M^+), 677, 501, 325. HPLC purity: normal phase SIL(M) column 100%; reverse phase C8 column 99.9%.

2.1.4. *(S,S)-α,ω-Bis{4-[(4′-(1-methylheptyloxycarbonyl)-4-biphenylyl)oxycarbonyl]phenoxy}nonane, (S,S)-BMHBOP-9*

α,ω-Bis-(4-carboxyphenoxy)nonane (**a–9**) (0.80 g, 2.0 mmol) and (*S*)-1-methylheptyl 4-hydroxybiphenyl-4′-carboxylate ((*S*)-**b**) (1.30 g, 4.0 mmol) were esterified using DMAP (0.05 g, 0.4 mmol) dry dichloromethane (10 ml) and DCC (1.23 g, 6.0 mmol) as described for BMHBOP-7. After removal of the solvent, the residue was purified by column chromatography using a dichrolomethane/hexane (5/1) mixture as eluent, and recrystallized from an ethanol/ethyl acetate (6/5) mixture, giving a colourless solid product; yield 1.08 g, (53%). δH (500 MHz, $CDCl_3$, TMS): 8.17 (m, 4H, Ar-**H**), 8.11 (m, 4H, Ar-**H**), 7.65 (m, 8H, Ar-**H**), 7.31 (m, 4H, Ar-**H**), 6.98 (m, 4H, Ar-**H**), 5.18 (m, 2H, $^{-}C^{*}\mathbf{H}(CH_3)^{-}$), 4.06 (t, 4H, $^{-}C\mathbf{H}_2O^{-}$, $^3J = 6.6$ Hz), 1.86 (m, 4H, $^{-}C\mathbf{H}_2CH_2O^{-}$), 1.75–1.30 (m, 36H, aliphatic-**H**), 0.88 (t, 6H, $^{-}C\mathbf{H}_3$, $^3J = 6.8$ Hz). ν/cm^{-1} (KBr): 2928, 2855 (C–H str.), 1734, 1702 (C=O str.), 1605 (C–C str.), 857 (1,4-disub. C–H o.o.p.d). m/z: 1016 (M^+), 691, 500, 325. HPLC purity: normal phase SIL(M) column 99.9%; reverse phase C8 column 99.8%.

2.1.5. *(S,S)-α,ω-Bis{4-[(4′-(1-methylheptyloxycarbonyl)-4-biphenylyl)oxycarbonyl]phenoxy}octane, (S,S)-BMHBOP-12*

α,ω-Bis-(4-carboxyphenoxy)dodecane (**a–12**) (0.88 g, 2.0 mmol) and (*S*)-1-methylheptyl 4-hydroxybiphenyl-4′-carboxylate ((*S*)-**b**) (1.30 g, 4.0 mmol) were esterified using DMAP (0.05 g, 0.4 mmol), in dry dichloromethane (10 ml) and DCC (1.23 g, 6.0 mmol). After removal of the solvent, the residue was purified by column chromatography using a dichrolomethane/hexane (10/3) mixture as eluent, and recrystallized from an ethanol/ethyl acetate (1/2) mixture, giving a colourless solid product; yield 1.11 g, (53%). δH (500 MHz, $CDCl_3$, TMS): 8.16 (m, 4H, Ar-**H**), 8.11 (m, 4H, Ar-**H**), 7.65 (m, 8H, Ar-**H**), 7.31 (m, 4H, Ar-**H**), 6.98 (m, 4H, Ar-**H**), 5.18 (m, 2H, $^{-}C^{*}\mathbf{H}(CH_3)^{-}$), 4.06 (t, 4H, $^{-}C\mathbf{H}_2O^{-}$, $^3J = 6.5$ Hz), 1.82–1.30 (m, 46H, aliphatic-**H**), 0.88 (t, 6H, $^{-}C\mathbf{H}_3$, $^3J = 6.9$ Hz). ν/cm^{-1} (KBr): 2921, 2853 (C–H str.), 1732, 1710 (C=O str.), 1607 (C–C str.), 845 (1,4-disub. C–H o.o.p.d). m/z: 1058 (M^+), 733, 529, 325. HPLC purity: normal phase SIL(M) column 100%; reverse phase C8 column 99.7%.

2.2. *Liquid crystalline and physical properties*

The initial phase assignments and corresponding transition temperatures for the final products were determined by thermal optical microscopy using a Nikon Optiphot-pol polarizing microscope equipped with a Mettler FP82 microfurnace and FP80 control unit. The heating and cooling rates were 2°C min^{-1} unless otherwise indicated. Temperatures and enthalpies of transition were investigated by differential scanning calorimetry (DSC) using a MAC Science MTC1000S calorimeter. The materials were studied at a scanning rate of 5°C min^{-1}, for both heating and cooling cycles, after being encapsulated in aluminium pans.

The X-ray scattering experiments were performed using a real-time X-ray diffractometer (Bruker AXS D8 Discover). The monochromatic X-ray beam (CuKα line) was generated by a 1.6 kW X-ray tube and Göbel mirror optics. The 2D position sensitive detector had 1024 × 1024 pixels in a 5 × 5 cm^2 beryllium window. A sample was introduced into a thin glass capillary (diameter 1.0 mm) and placed in a custom-made temperature stabilized holder (stability within ±0.1°C).

Electro-optical studies were carried out using commercially available evaluation cells (purchased from E.H.C. Co. Ltd., Japan). The cells were made with 3 μm spacings and the inner surfaces had been coated with a polyimide (PI) aligning agent and unidirectionally buffed. The optical tilt angle (defined as the angle between the layer normal in the smectic phases and the extinction direction when the sample is rotated during polarizing light microscopy) was determined by finding the extinction direction when an electric field was applied to the specimen in increasing or decreasing steps. A Kikusui Electric Regulated DC Power Supply was used to supply the d.c. field.

3. Results

3.1. *Phase transition behaviour*

Phase transition temperatures for the homologous series of chiral twins BMHBOP-*n* are listed in table 1, and are also compared schematically in figure 2. All of the homologues studied here favoured the antiferroelectric and/or ferrielectric phase rather than the ferroelectric phase but, did not show the smectic A* phase. BMHBOP-8 and BMHBOP-12 exhibited a chiral nematic phase, showing the typical oily-streak texture, whereas BMHBOP-6, BMHBOP-7 and BMHBOP-9 showed no chiral nematic phase. Figure 3 shows the textural change obtained for BMHBOP-8 at the chiral nematic–ferrielectric phase transition observed using the polarized light microscope. Pseudo-homeotropic alignment of the ferrielectric phase gave dark round-shaped domains in the oily-streak texture of the chiral nematic phase. With decreasing temperature, a characteristic

Table 1. Phase transition temperatures (°C), transition enthalpies (kJ mol^{-1}) (in square brackets), and entropies (R) (in italics) for the homologous series BMHBOP-*n*.

n	Absolute configuration	cryst.		antiferro		ferri		ferro		N*		I	Diffuse peak[a]
6	(*S*,*S*)	•	135.7 [51.50] *15.16*	•	159.7 [0.44] *0.12*	•	178.7 [-][b]	•		—	179.3 [2.57][b] *0.68*	•	[2.64]
6	(*R*,*R*)	•	137.3 [55.04] *16.13*	•	159.7 [0.48] *0.13*	•	178.1 [-][b]	•		—	178.7 [2.57][b] *0.68*	•	[2.83]
7	(*S*,*S*)	•	109.1 [42.74][c] *13.45*	•	112.3 [-][d]	•		—		—	113.2 [5.37][d] *1.67*	•	—[e]
8	(*S*,*S*)	•	139.3 [59.18] *17.26*	•	141.8 [0.64] *0.19*	•		—	147.7 [6.28] *1.80*	•	156.7 [0.17] *0.05*	•	[1.37]
8	(*R*,*R*)	•	140.9 [54.28] *15.77*	•	140.9 [0.59] *0.17*	•		—	146.6 [5.65] *1.62*	•	155.3 [0.13] *0.04*	•	[1.29]
9	(*S*,*S*)	•	109.1 [56.57][c] *17.81*	•		—		—		—	(102.5)[f] [-][g]	•	—[e]
12	(*S*,*S*)	•	113.8 [60.45] *18.80*	•		—		—	(109.9)[f] [11.10] *3.49*	•	129.8 [0.28] *0.08*	•	[0.73]

[a] A broad diffuse DSC peak appeared in the isotropic liquid phase.
[b] Peaks corresponding to the ferri–ferro and ferro–I transitions were not separated clearly, and therefore only the total of the enthalpy values for the two transitions were measured.
[c] Measured on the second heating cycle.
[d] Peaks corresponding to the anti–ferri and ferri–I transitions were not separated clearly, and therefore, only the total of the enthalpy values for the two transitions were measured.
[e] A broad DSC peak in the I phase did not appear.
[f] () indicates a monotropic phase transition.
[g] The transition enthalpy could not be obtained due to the occurrence of immediate recrystallization.

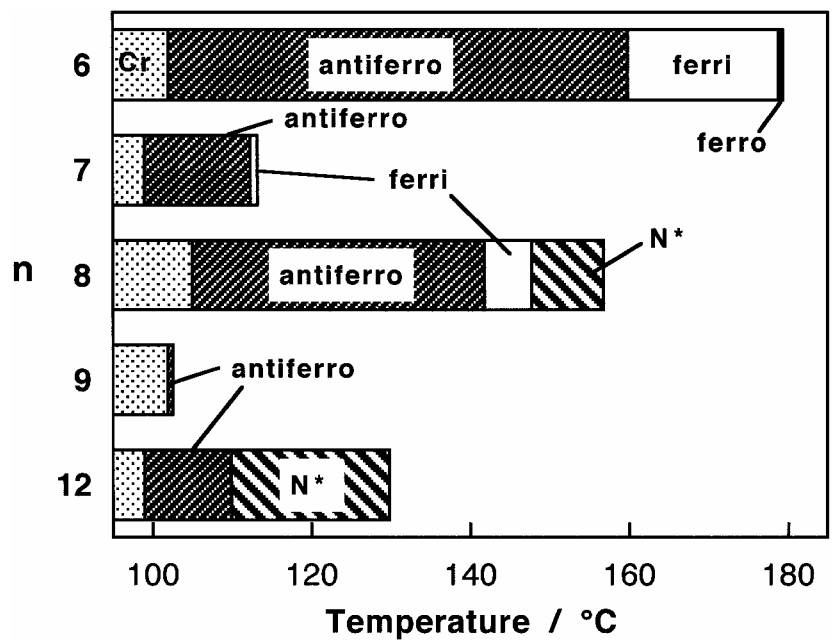

Figure 2. Phase transition temperatures for BMHBOP-*n*.

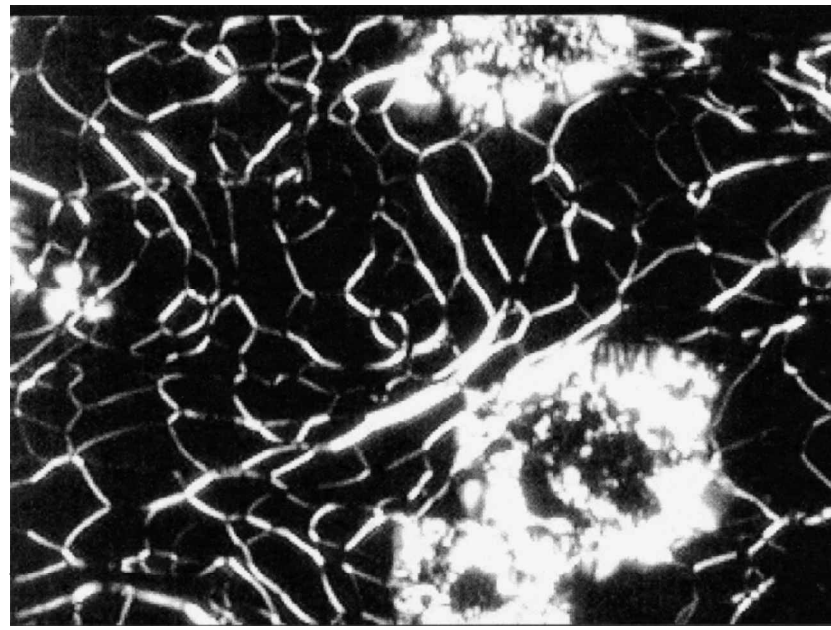

Figure 3. Optical texture observed at the chiral nematic–ferrielectric phase transition of BMHBOP-8.

texture with constant movement, similar to that reported for the ferrielectric phase of the analogous monomer [13], was observed. Thus, BMHBOP-8 was found to show the ferrielectric and antiferroelectric phases with a broad temperature range chiral nematic phase (*c.* 10°C). With increasing alkyl spacer length, the temperature range of the ferrielectric phase became narrow and the ferrielectric phase disappeared for BMHBOP-12, whereas the chiral nematic phase range became wider. As a result, BMHBOP-12 showed the antiferroelectric phase with a broad temperature range (*c.* 20°C) of chiral nematic phase.

With increasing alkyl spacer length, the clearing point decreased with a strong odd–even effect. The odd-membered homologues showed substantially weaker liquid crystallinity than the even members. BMHBOP-7 showed the antiferroelectric phase with a narrow temperature range (*c.* 1°C) of ferrielectric phase. BMHBOP-9 showed the antiferroelectric phase, but this phase was monotropic and the temperature range of the antiferroelectric phase formed on cooling was quite narrow (less than 1°C) due to the occurrence of recrystallization.

3.2. *Differential scanning calorimetry studies*

Figure 4 shows differential scanning calorimetry (DSC) thermograms for the homologues. The transition enthalpies and entropies associated with the transition temperatures are summarized in table 1. DSC peaks corresponding to the ferri–ferro and ferro–isotropic transitions for BMHBOP-6 were not separated clearly, but a shoulder corresponding to the ferri–ferro transition was observed as shown in figure 4 (*a*). At the antiferro–ferri transition of BMHBOP-6, a sharp peak was observed, indicating that the transition is first order in nature. A broad DSC peak appeared in the isotropic liquid phase of BMHBOP-6. Similarly, BMHBOP-8 and BMHBOP-12 showed a broad diffuse DSC peak in the isotropic liquid region, but the peak became broader and weaker on increasing the central spacer length, figures 4 (*c*) and 4 (*d*). The DSC peak that appeared in the isotropic region of BMHBOP-12 was quite broad and low, but the existence of the peak was confirmed in repeated heating and cooling cycles of DSC measurements. The odd-membered homologues, i.e. BMHBOP-7 and BMHBOP-9, did not exhibit a broad diffuse peak in the isotropic liquid phase. A shoulder appeared on the DSC thermogram and corresponded to the ferri–antiferro transition of BMHBOP-7, see figure 4 (*b*).

3.3. *Miscibility studies*

Miscibility studies were performed between the homologues so that a consistent assignment of the phases could be achieved. Figure 5 shows a phase diagram for mixtures between BMHBOP-8 and BMHBOP-6. The phase diagram shows continuous miscibility across the full composition range between BMHBOP-8 and BMHBOP-6 for the antiferroelectric and for the ferrielectric phases. Similarly, figure 6 shows a phase diagram between BMHBOP-8 and BMHBOP-12 showing continuous miscibility across the full composition range for the antiferroelectric phase, so that the phase sequence of BMHBOP-12 was confirmed as 'isotropic liquid–chiral nematic–antiferro'. A phase diagram was also obtained between BMHBOP-8 and BMHBOP-7 as shown in figure 7. The antiferroelectric and ferrielectric phases were found to be individually miscible.

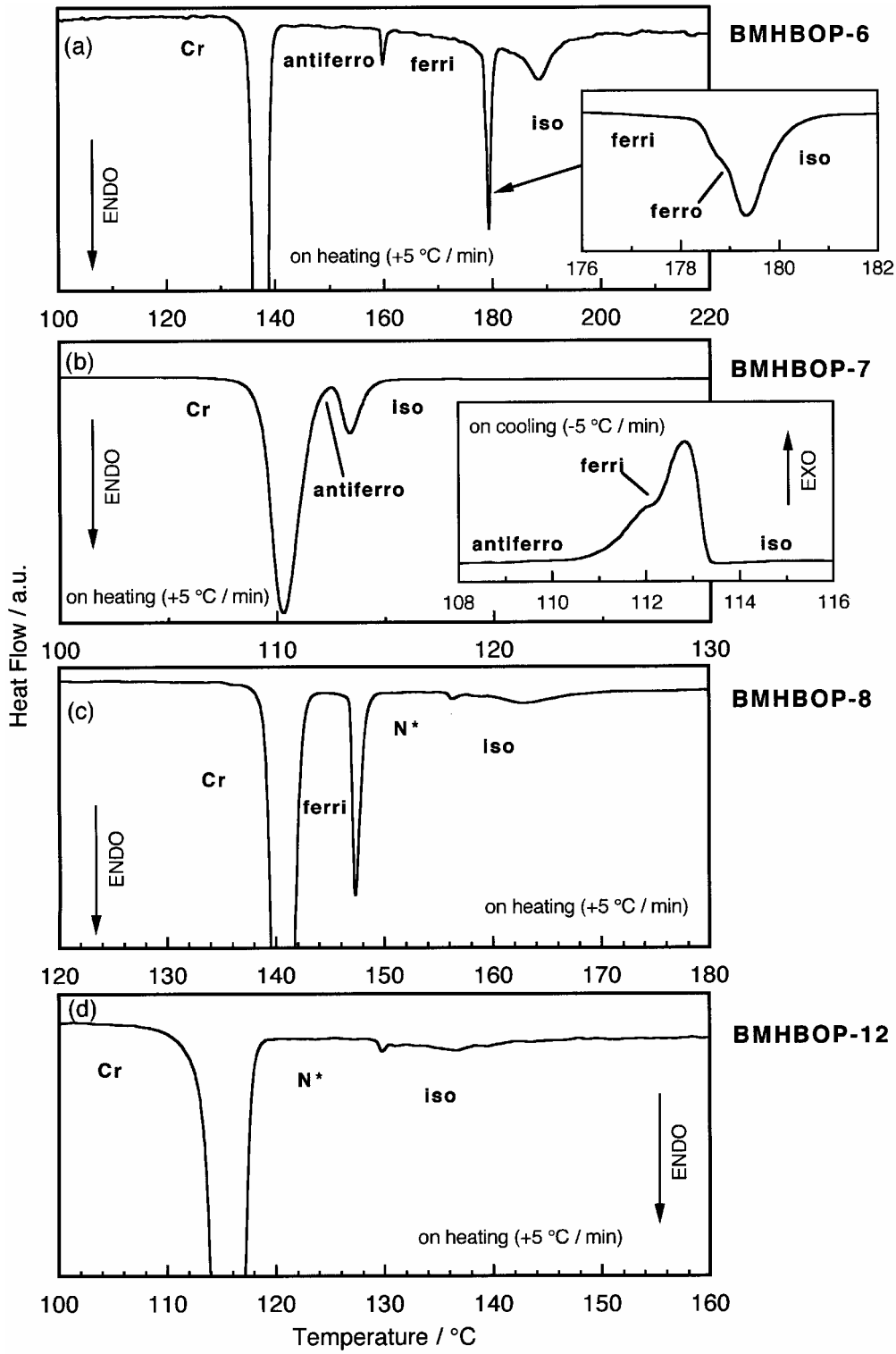

Figure 4. DSC thermograms of BMHBOP-n.

3.4. *X-ray diffraction studies*

Figure 8 shows intensity profiles of the wide angle X-ray scattering for the homologous series of chiral twin compounds BMHBOP-n, together with that obtained for the analogous monomeric compound 10B1M7 [13] (see figure 9). The twin homologues showed sharp first and second order peaks in the small angle region corresponding to the smectic layer spacing, whereas the

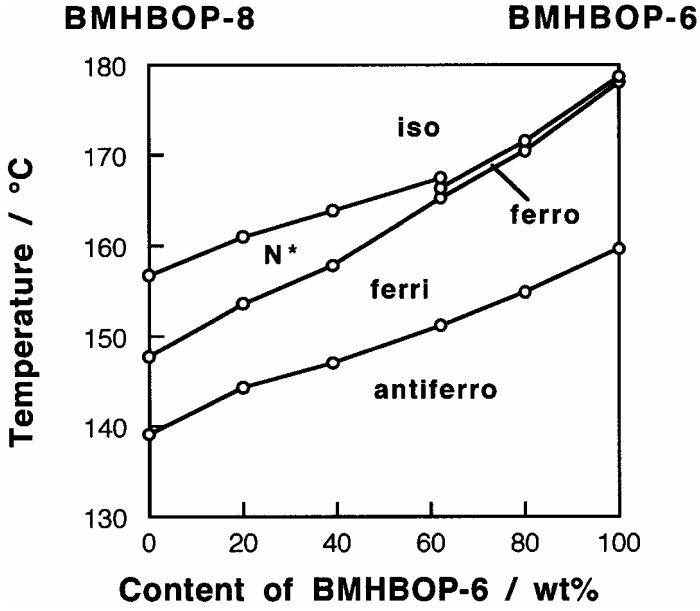

Figure 5. Miscibility phase diagram between BMHBOP-8 and BMHBOP-6.

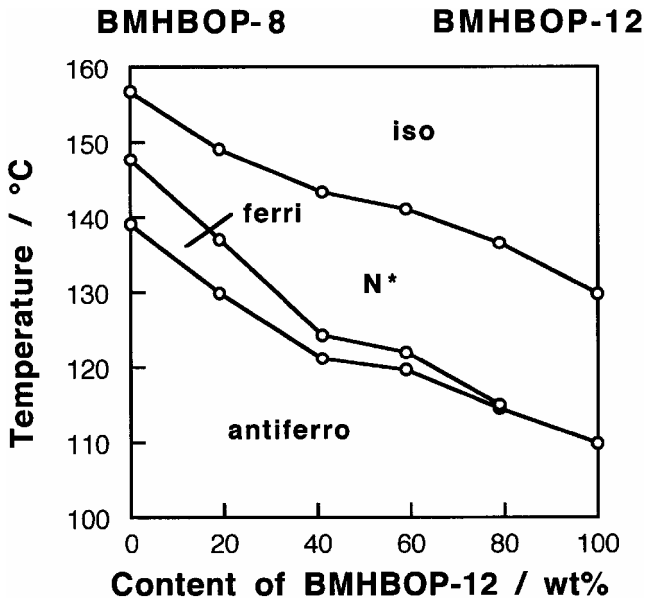

Figure 6. Miscibility phase diagram between BMHBOP-8 and BMHBOP-12.

analogous monomer showed only one sharp peak corresponding to the smectic layer spacing. In particular, BMHBOP-12 showed a significantly larger second order peak. The appearance of the second order peak for BMHBOP-n indicates the formation of a relatively well defined smectic layer structure which is considered to be important for generating anticlinic structures in the ferrielectric and antiferroelectric phases. The molecular structure also has an important e^{ff}ect on determining

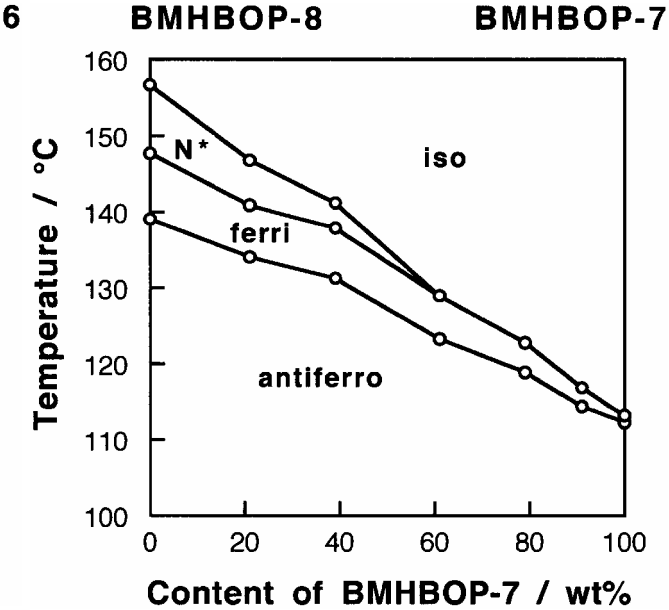

Figure 7. Miscibility phase diagram between BMHBOP-8 and BMHBOP-7.

the strength of the second order reflection which may be, in the case of BMHBOP-12 because the length of the central spacer is roughly twice the length of the peripheral chain. Di^{ff}use scattering in the wide angle region was observed for all of the smectic phases of the homologues, indicating that there is no long range positional order within the layers. This indicates that the antiferroelectric, ferrielectric and ferroelectric phases are in fact sub-phases of the smectic C* phase. Interestingly, even in the isotropic phase near to the smectic–isotropic phase transitions of BMHBOP-6 and BMHBOP-7, a clear XRD peak was observed in the small angle region as shown in figure 10, whereas the monomer 10B1M7 showed no such peak. The XRD peak obtained in the small angle region of BMHBOP-6 and BMHBOP-7 showed a lower angle shift at the transition from the smectic to the isotropic phase, as shown in figures 10 (^{a}) and 10 (^{b}), respectively, whereas 10B1M7 showed a higher angle shift, see figure 10 (^{c}).

Figure 11 shows the temperature dependence of the layer spacing in the smectic phase, or the length corresponding to the local or short range transitional correlation in the isotropic phase, which was calculated from the positions of the sharp peak in the small angle region, obtained for BMHBOP-n and 10B1M7, together with the peak intensities. BMHBOP-6 and BMHBOP-7 showed similar profiles for the layer spacing, i.e. the layer spacing increases toward the transition form the smectic phase to the isotropic phase. In the isotropic phase, however, the length corresponding to the local or short range transitional correlation decreases with

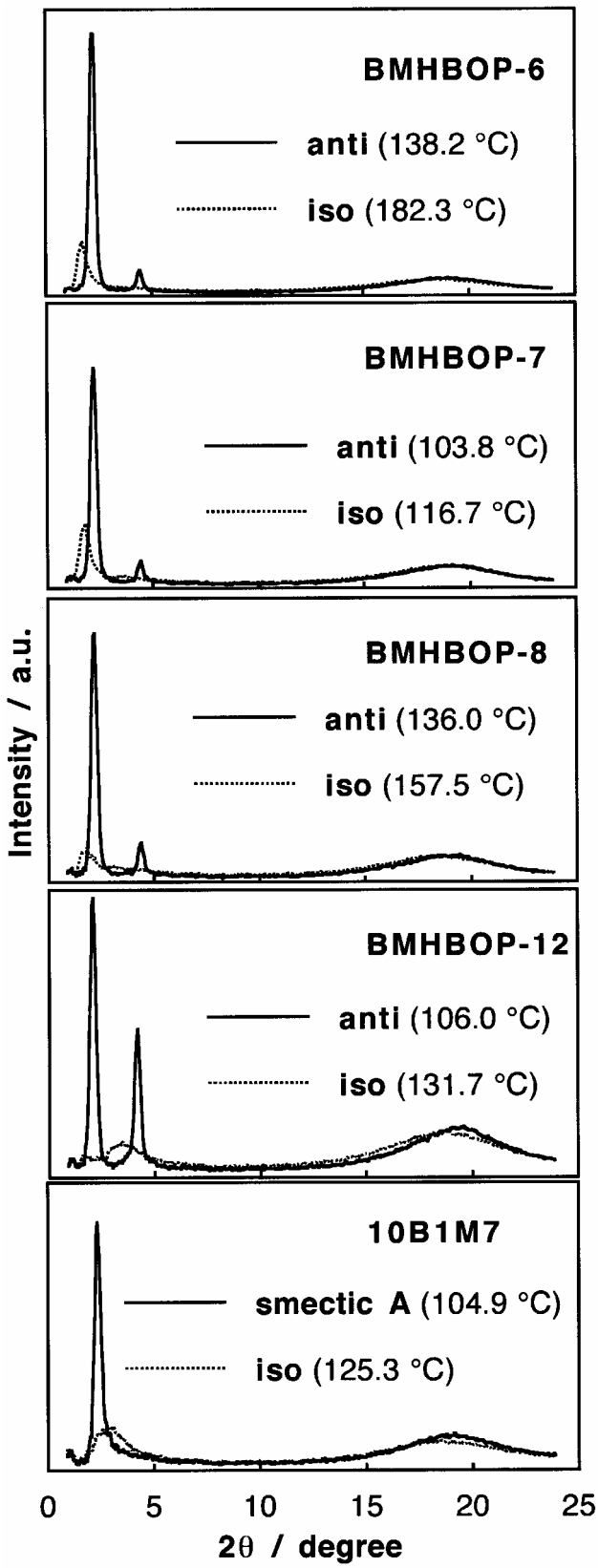

Figure 8. X-ray scattering patterns of BMHBOP-n and the analogous monomer, 10B1M7.

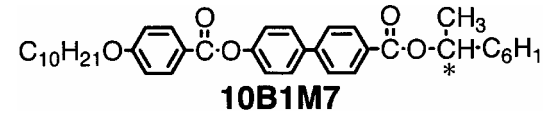

Figure 9. Structure of 10B1M7.

increase in temperature. The intensity of the X-ray scattering peak that appeared in the small angle region decreased suddenly at the smectic–isotropic phase transition, but certain values of the peak intensities were still clearly obtained just above the smectic–isotropic transition. BMHBOP-8 showed that the layer spacing increases at the ferrielectric–chiral nematic transition and then decreases with increasing temperature. However, BMHBOP-12 showed a totally different tendency for the temperature dependence of the layer spacing, i.e. the spacing decreased at the transition from the antiferroelectric to chiral nematic phase; the intensity also decreased at the transition. The profile obtained for BMHBOP-12 is somewhat similar to that obtained for the monomeric analogue 10B1M7, figure 11 (*e*).

3.5. *Electro-optical studies*

Figure 12 shows the applied electric field dependence of the optical tilt angle in the ferroelectric, ferrielectric and antiferroelectric phases of BMHBOP-6. In the ferroelectric phase, a good bistability with a large tilt angle of 52° was observed. In the ferrielectric phase, a characteristic multi-step change in the tilt angle was obtained with a large saturated tilt angle of 46°, corresponding to the electrically induced ferroelectric state. It should be noted that a metastable plateau corresponding to the ferrielectric ordering also showed a large tilt angle of 40°. In the ferrielectric phase of BMHBOP-6, clear textural changes on applying the electric field were observed for the homogeneously aligned sample; figure 13 (*a*) shows a texture without the electric field, and figures 13 (*b*) and 13 (*c*) show the textures corresponding to the metastable ferrielectric ordering and to the electrically induced ferroelectric state, respectively. In the antiferroelectric phase, a characteristic threshold behaviour with a rather large pre-transitional effect was observed, where a large saturated tilt angle of 52°, corresponding to the induced ferroelectric ordering, was obtained.

The applied electric field dependence on the optical tilt angle at the ferrielectric and antiferroelectric phases of BMHBOP-7 is shown in figure 14. The characteristic multi-step change in tilt angles was observed in the ferrielectric phase, figure 14 (*a*). The antiferroelectric phase of BMHBOP-7 showed a d.c. threshold electric field of 9 MV m^{-1}, with a large pretransitional effect where the co-existence of the antiferroelectric and the induced ferroelectric domains was observed, figure 14 (*b*). Figure 15 shows the multi-step tilt angle change as a function of

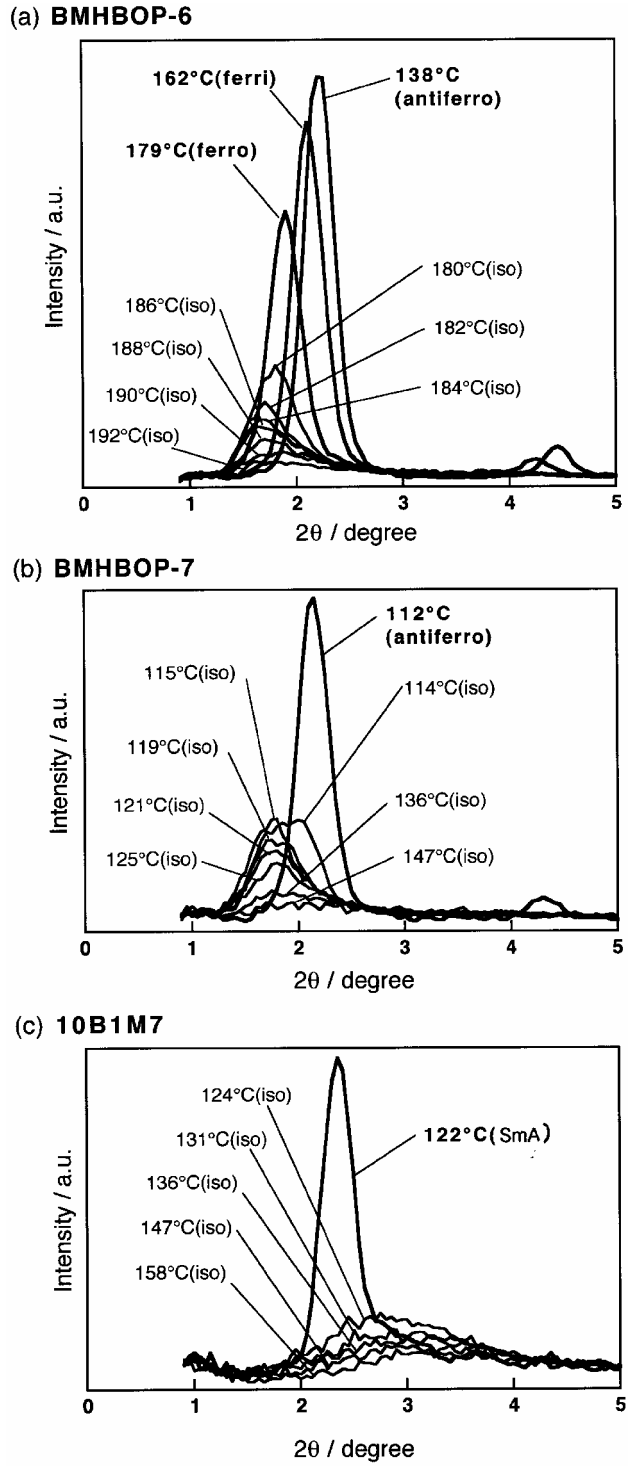

Figure 10. X-ray scattering patterns obtained around the smectic–isotropic phase transition for BMHBOP-6, BMHBOP-7 and 10B1M7.

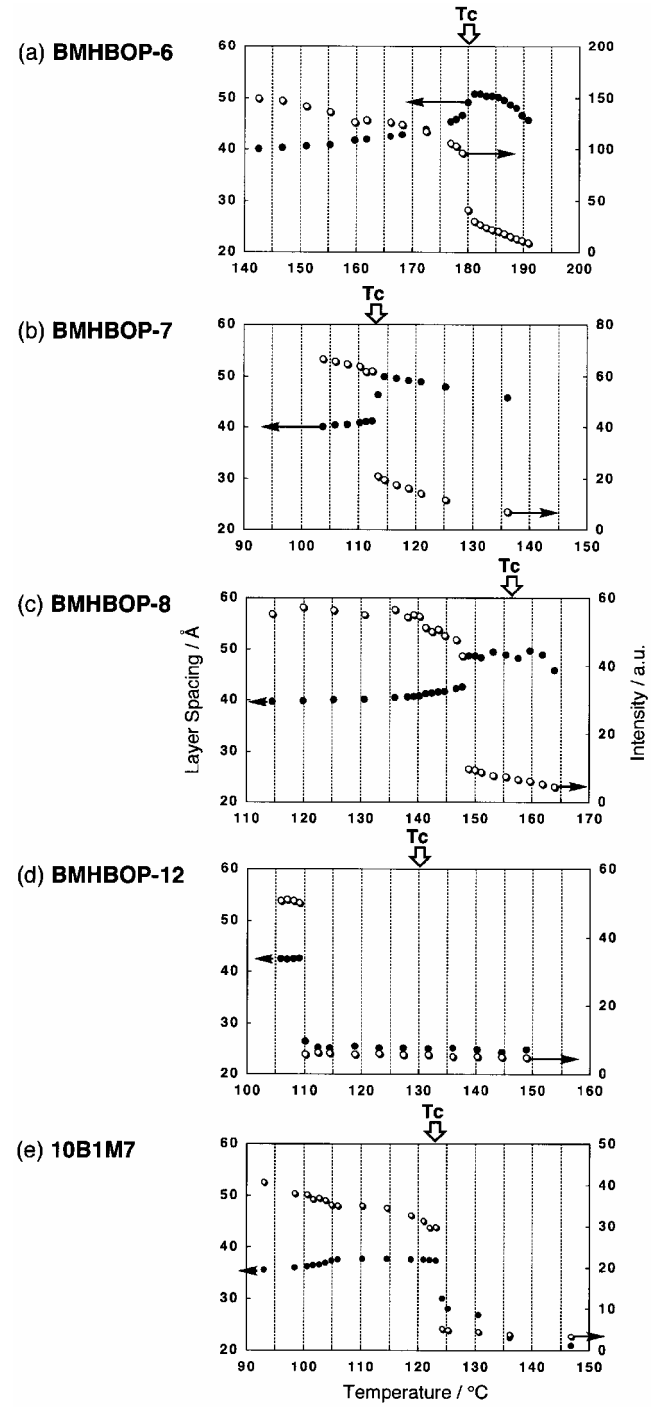

Figure 11. Layer spacings and intensities as a function of temperature for BMHBOP-n and 10B1M7 (T_c = clearing temperature).

the applied electric field observed in the ferrielectric phase of BMHBOP-8. The saturated tilt corresponding to the electrically induced ferroelectric ordering showed a large angle of 50°. The metastable plateau with respect to the ferrielectric ordering also showed a large angle of 42°. Since BMHBOP-9 and BMHBOP-12 showed only a monotropic antiferroelectric phase, detailed tilt angle measurements could not be performed due to the occurrence of recrystallization during the measurements.

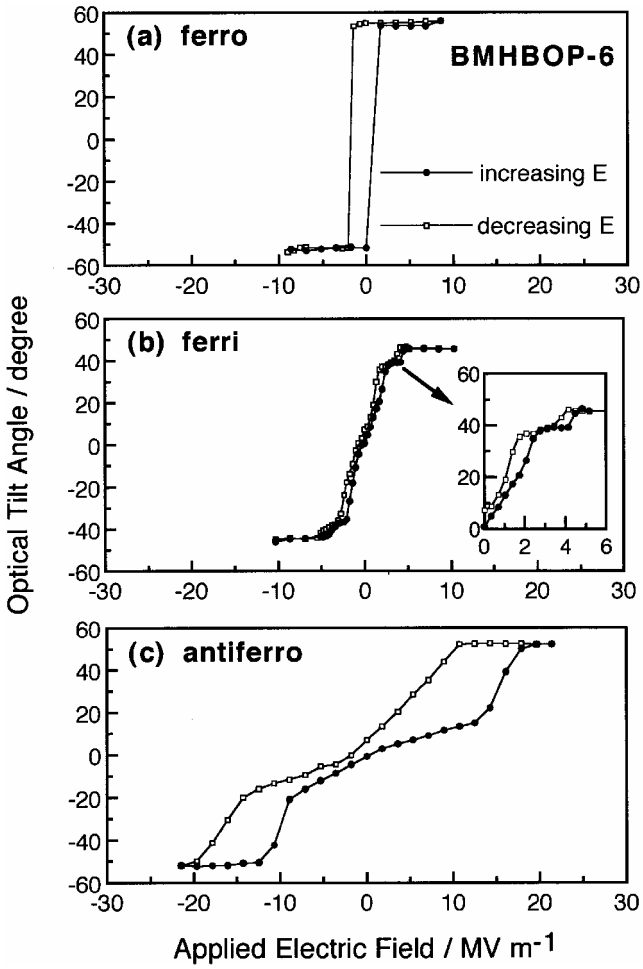

Figure 12. Optical tilt angle as a function of the applied electric field for the (*a*) ferroelectric, (*b*) ferrielectric and (*c*) antiferroelectric phases of BMHBOP-6.

However, the characteristic threshold behaviour, which is typical for the antiferroelectric phase, was confirmed by rapid application of a d.c. electric field to the sample. The tilt angle of BMHBOP-12 in the antiferroelectric phase, just below the chiral nematic–antiferroelectric phase transition, was found to be 52°.

3.6. *Effect of optical activity*

(*S*,*S*)- and (*R*,*R*)-BMHBOP-6 showed a bizarre diffuse peak in the isotropic liquid region, see figure 4 (*a*). However, a 1 : 1 mixture of the two optical isomers showed no diffuse peak in the DSC thermogram, but a sharp peak corresponding to a nematic–isotropic liquid transition, even though the (*S*,*S*)- and (*R*,*R*)-isomers themselves do not exhibit chiral nematic phases. The emergence of the nematic phase was also confirmed by contact preparation studied. Figure 16 shows a photomicrograph of the contact region between the (*S*,*S*)- and (*R*,*R*)-isomers at 186°C as observed using the polarizing

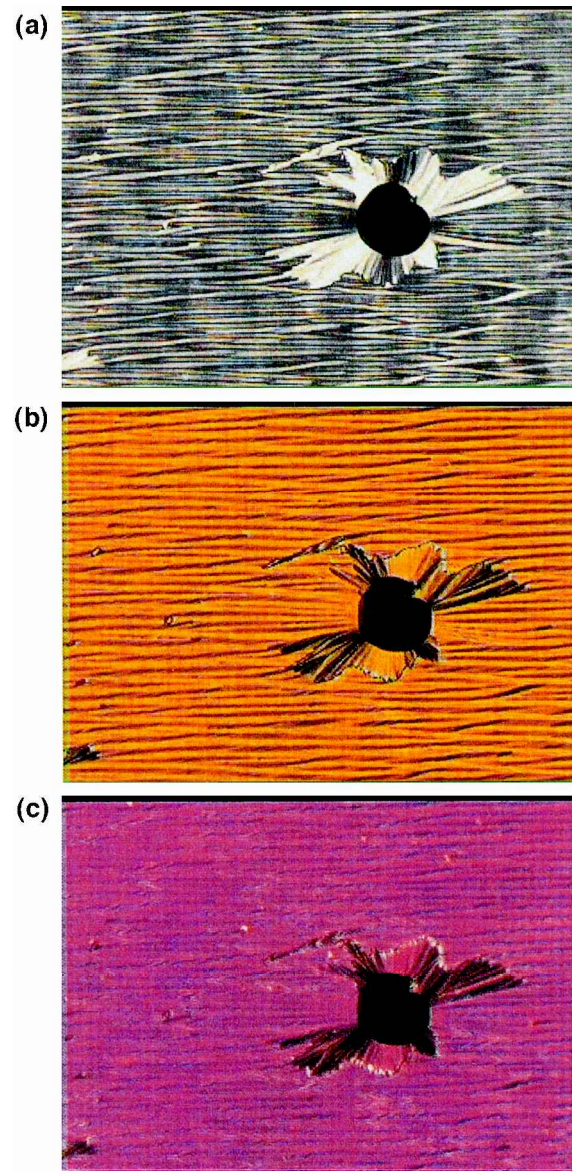

Figure 13. Optical texture change on application of an electric field in the ferrielectric phase of BMHBOP-6; (*a*) 0 V μm^{-1}, (*b*) 3.4 V μm^{-1} (ferrielectric ordering) and (*c*) 5.2 V μm^{-1} (induced ferroelectric ordering).

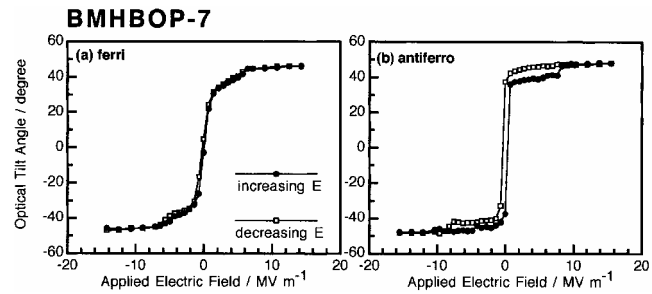

Figure 14. Optical tilt angle as a function of the applied electric field for the (*a*) ferrielectric and (*b*) antiferroelectric phases of BMHBOP-7.

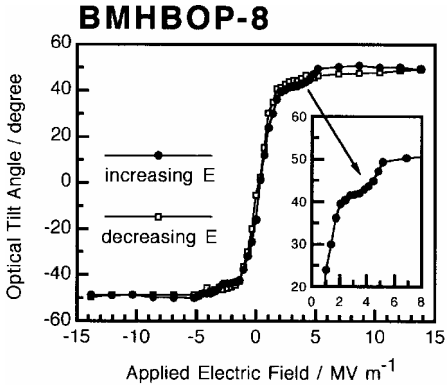

Figure 15. Optical tilt angle as a function of the applied electric field for the ferrielectric phase of BMHBOP-8.

light microscope. The (*S*,*S*)- and (*R*,*R*)-isomers show the isotropic phase at 186°C as totally dark regions, but the chiral nematic phase is seen to be induced around the contact area. The schlieren texture of the nematic phase was observed at the central contact region where the pitch of the chiral nematic phase became compensated. The DSC thermograms for (*S*,*S*)-BMHBOP-8, (*R*,*R*)-BMHBOP-8 and the 1:1 mixture of the two optical isomers are shown in figure 17. As stated above, a broad peak appeared in the isotropic phase of (*S*,*S*)- or (*R*,*R*)-BMHBOP-8, but this was not observed for the 1:1 mixture for which a sharp peak appeared corresponding to the nematic–isotropic liquid transition.

4. Discussion

The calculated molecular length (l), the optical tilt angle (θ), the values of '$l \times \cos\theta$', and the layer spacing (d) obtained from the X-ray scattering experiments are summarized in table 2. All of the homologues studied showed that the '$l \times \cos\theta$' values are comparable to the layer spacings, which strongly suggests that the homologues form a monolayered structure rather than an intercalated structure. If this is the case, then the two mesogenic groups of each twin molecule form a 'pseudo' bilayer structure which allows the chiral moieties to lie in proximity to the interfaces of the smectic layers; the chiral interactions between layers are therefore expected to be relatively strong in comparison to monomeric systems. The differences between the '$l \times \cos\theta$' values and the observed layer spacings may be attributed to the difference between the optical tilt used for the calculation and the real steric molecular tilt [14, 15].

The observed tendency to form a monolayered structure for BMHBPO-n agrees with the reported results that symmetric dimers generally form a monolayered smectic phase [16], although a few exceptions have been reported [17]. The result obtained indicates that microphase separation [16, 18], giving three distinct regions containing either mesogenic cores, alkyl central spacers or terminal chains, occurs in this homologous series. With increasing central spacer length, the stability of the chiral nematic phase increased, which is again similar to the reported behaviour for many dimer series [16]. Thus, the molecular design of introducing into the peripheral

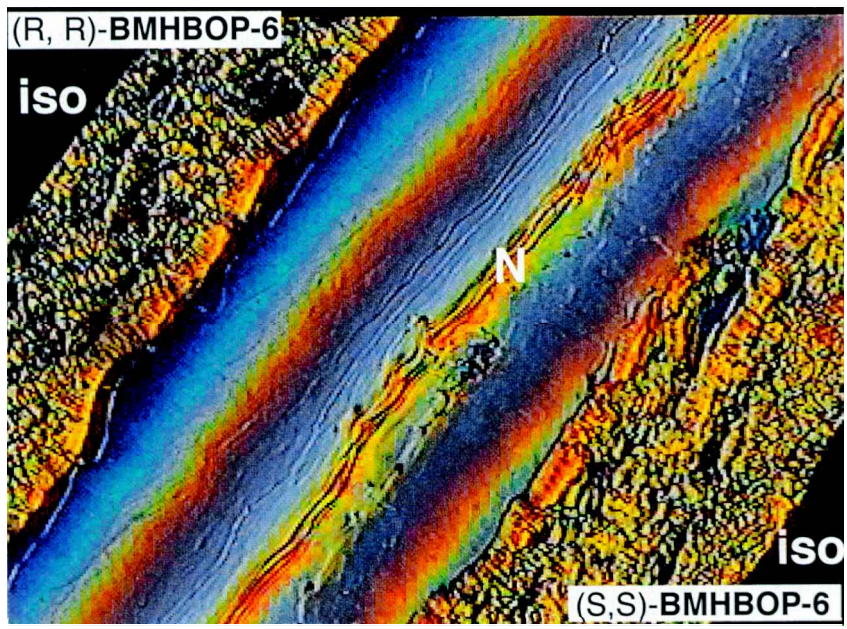

Figure 16. Optical texture obtained for the contact preparation between (*S*,*S*)- and (*R*,*R*)-BMHBOP-6 at 186°C.

Table 2. Molecular length l, saturated tilt angle θ, and estimated and observed layer spacings for BMHBOP-n.

Compound	Mesophase	l/Å[a]	θ/°[b]	Estimated layer spacing (l × cos θ)/Å[c]	Observed layer spacing (d)/Å[d]
BMHBOP-6	ferri	57.5	45.1	40.6	42.5
	antiferro		47.8	38.6	40.6
BMHBOP-7	ferri	56.3	46.2	39.0	41.1
	antiferro		47.7	37.9	40.8
BMHBOP-8	ferri	60.1	48.9	39.5	41.7
	antiferro		50.3	38.4	40.7
BMHBOP-12	antiferro	64.8	52.4	39.5	42.5

[a] Estimated by MM2 calculation.
[b] Optical apparent tilt angle measured using the polarizing light microscope.
[c] Estimated from the molecular length (l) and the saturated tilt angle (θ), under the assumption that the twin molecules form a 'monolayered' structure.
[d] Calculated from the X-ray diffraction peak that appeared in the small angle region.

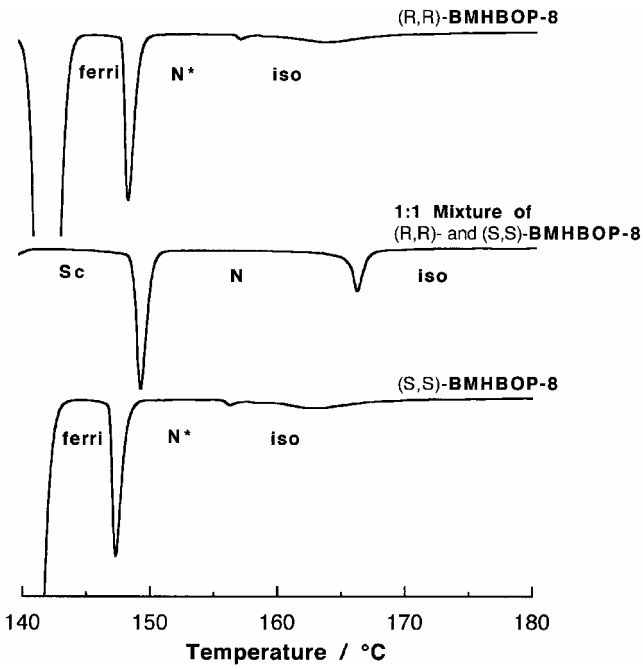

Figure 17. Comparison of DSC thermograms between (*S*,*S*)-BMHBOP-8, (*R*,*R*)-BMHBOP-8 and the 1:1 mixture of the optical isomers.

ends of a symmetric twin configuration chiral moieties that favour generation of antiferroelectric and ferrielectric molecular assemblies, allows us to obtain antiferroelectric and ferrielectric materials possessing a chiral nematic phase. It is interesting that BMHBOP-12 also showed a monolayered smectic structure, because the length of the terminal chain of BMHBOP-12 is roughly half the length of the central spacer. It has been reported that for smectic properties to be observed in many cases of symmetric twins, the length of the terminal chains must be greater than half the length of the spacer [16]. The case of BMHBOP-12 seems to be critical for this condition. The segregation effect produced in the BMHBOP homologues may be strong enough to form a monolayered structure.

BMHBOP-6 and BMHBOP-8 showed a stable ferrielectric phase, but the related twin homologues possessing two identical chiral moieties in the 'inner' region of the molecular structure (see figure 18) have been reported not to exhibit the ferrielectric phase, but instead to exhibit ferroelectric and antiferroelectric phases [19]. These results indicate that the position of the chiral moieties in the overall structure is quite important for the appearance of the ferrielectric phase. i.e. the chiral moieties located at the peripheral ends of the BMHBOP-n molecules promote the interaction between smectic layers that stabilizes the ferrielectric character. With increasing central spacer length, the temperature range of the ferrielectric phase was reduced, indicating that the coupling in motion and/or direction between two mesogenic parts also plays an important role in the stabilization of the ferrielectric phase.

It should be noted that the metastable tilt angle obtained for the ferrielectric ordering is quite large compared with the saturated tilt angle of the induced ferroelectric ordering as shown below:

BMHBOP-6 (ferrielectric tilt = 40°, saturated tilt = 46°);
BMHBOP-8 (ferrielectric tilt = 42°, saturated tilt = 50°).

The structures of the ferrielectric phase have so far been proposed to consist of three- or four-layer repeating units [19*b*), 1(*c*), 20]. However, the large tilt angle

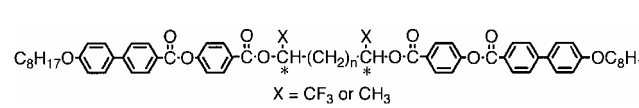

Figure 18. Chiral twin compound possessing chiral centres in the 'inner' part of the overall molecular structure.

obtained for the ferrielectric orderings of the chiral twins BMHBOP-6 and BMHBOP-8 cannot be explained by only three or four repeating units. If the ferrielectric phase of BMHBOP-6 were formed by a three-layer repeating unit, the expected ferrielectric tilt would be only $[46 \times (2) + 46 \times (-1)]/3 = 15^{\circ}$. In order to obtain the observed large ferrielectric tilt angle, approximately ten layers are required in one repeating unit. Thus, the ferrielectric structures obtained for the chiral twins studied here are believed to be produced by longer range interactions between smectic layers than for usual monomeric systems.

Finally, let us consider the isotropic–isotropic liquid transition observed for the even-membered BMHBOP-*n*. The two isotropic phases show completely dark textures under examination using polarized light microscopy. However, as noted earlier (see figure 4), a bizarre diffuse peak above the smectic–isotropic liquid transition was observed in the DSC thermograms. It should be noted that the lower temperature isotropic phase is totally different from the chiral nematic phase, because a small but clear DSC peak was obtained for the chiral nematic–isotropic phase transition, see figures 4(*c*) and 4(*d*). Since only the even-membered homologues showed the iso–iso transition, the molecular packing responsible for the emergence of the unusual isotropic phase may be stabilized by the straight shaped conformation of twin molecules. The transitional entropies of the chiral nematic–isotropic liquid transition were found to be quite small, having values in the range 0.04 to 0.08 R, compared with the values so far reported for traditional twins [16]. However, when a broad DSC diffuse peak appears in the isotropic region, the DSC peak associated with the clearing point has been reported to become small [21(*a*)], thus providing smaller entropies than usual. These small entropy values could indicate that the isotropic phase just above the clearing temperature still possesses an organized structure to some extent.

So far, the appearance of the broad diffuse DSC peak in the isotropic region has been reported for some compounds showing a TGB phase [21] or a cubic phase [22], but this behaviour has not been reported for the monomeric analogue [13] of BMHBOP-*n*. The broad diffuse DSC peak observed for the twin homologues became broader and weaker with increasing central spacer length, which is consistent with the fact that the monomeric character of the twin homologues increases with increasing central spacer length. The structures of these isotropic phases are not fully understood at present. However, such broad DSC peaks can be found when there is a continuous change in structure as well as a phase transition. Therefore similar behaviours to the lattice melting process so far proposed [23] could also occur in the chiral twin system studied here. The disappearance of the broad peak in the isotropic phase of (*S*,*S*)- and of (*R*,*R*)-BMHBOP in a 1:1 mixture, as described earlier, is also intriguing.

5. Conclusions

Octyl and dodecyl homologues of chiral twin liquid crystals possessing identical chiral moieties at both peripheral ends, i.e. optically active α,ω-bis{4-[(4′-(1-methylheptyloxycarbonyl)-4-biphenylyl)oxycarbonyl]phenoxy}-alkanes, were found to be the first ferrielectric and/or antiferroelectric materials to show a broad (more than 10°C) chiral nematic phase. The twin homologues favoured formation of a monolayered smectic structure which allows the chiral groups to interact with each other at the interfaces between the planes of the smectic layers, producing stronger chiral interactions between the neighbouring smectic layers. Thus, the chirality-induced superstructure of the ferrielectric ordering became stabilized. Correlation between the two mesogenic parts in each molecule also played an important role in the stabilization of the ferrielectric phase.

We wish to thank Professor J. Watanabe, Tokyo Institute of Technology, for valuable discussions, and also Dr R. A. Lewis, Hull University, for supplying the monomeric compound.

References

[1] For example: (*a*) Miyachi, K., and Fukuda, A., 1998, *Handbook of Liquid Crystals*, Vol. 2B, edited by D. Demus, J. W. Goodby, G. W. Gray, H.-W. Spiess and V. Vill (Weinheim: Wiley-VCH), pp. 665–691; (*b*) Takezoe, H., and Takanishi, Y., 2001, *Chirality in Liquid Crystals*, edited by H.-S. Kitzerow and C. Bahr (New York: Springer-Verlag), pp. 251–295; (*c*) Matsumoto, T., Fukuda, A., Johno, M., Motoyama, Y., Yui, T., Seong, S.-S., and Yamashita, M., 1999, *J. mater. Chem.*, **9,** 2051; (*d*) Fukuda, A., Takanishi, Y., Isozaki, T., Ishikawa, K., and Takezoe, H., 1994, *J. mater. Chem.*, **4,** 997; (*e*) Nishiyama, I., 1994, *Adv. Mater.*, **6,** 966.

[2] See for example: Geelhaar, T., 1988, *Ferroelectrics*, **85,** 329.

[3] D'have, K., Rudquis, P., Lagerwall, S. T., Pauwels, H., Drzewinski, W., and Dabrowski, R., 2000, *Appl. Phys. Lett.*, **76,** 3528.

[4] Aoki, Y., and Nohira, H., 1999, *Liq Cryst.*, **26,** 97.

[5] Yoshizawa, A., Ise, N., and Okada, T., 1998, *Ferroelectrics*, **214,** 75.

[6] Tashiro, K., Hou, J.-A., and Kobayashi, M., 1994, *Macromolecules*, **27,** 3912.

[7] Nishiyama, I., Yamamoto, J., Goodby, J. W., and Yokoyama, H., 2001, *J. mater. Chem.*, **11,** 2690.

[8] Nishiyama, I., Yamamoto, J., Goodby, J. W., and Yokoyama, H., 2001, *Helical structures produced in some binary mixtures between twin and monomeric liquid crystals* (P-14), presented at the Second Anglo-Japanese Seminar on Liquid Crystals. 5–7 September, 2001, York, UK.

[9] Hassnei, A., and Alexanian, V., 1978, *Tetrahedron. Lett.*, 4475.
[10] (*a*) Griffin, A. C., and Havens, S. J., 1981, *J. polym. Sci. polym. Phys.*, **19,** 954; (*b*) Donahoe, H. B., Benjamin, L. E., Fennoy, L. V., and Greiff, D., 1961, *J. org. Chem.*, **26,** 474.
[11] Chin, E., and Goodby, J. W., 1986, *Mol. Cryst. liq Cryst.*, **141,** 311.
[12] Mitsunobu, O., 1981, *Synthesis*, 1.
[13] Goodby, J. W., Patel, J. S., and Chin, E., 1992, *J. mater. Chem.*, **2,** 197.
[14] Goodby, J. W., Chin, E., Leslie, T. M., Geary, J. M., and Patel, J. S., 1986, *J. Am. chem. Soc.*, **108,** 4729.
[15] Mills, J. T., Gleeson, H. F., Goodby, J. W., Hird, M., Seed, A., and Styring, P., 1998, *J. mater. Chem.*, **8,** 2385.
[16] (*a*) Imrie, C. T., and Luckhurst, G. R., 1998, *Handbook of Liquid Crystals*, Vol. 2B, edited by D. Demus, J. W. Goodby, G. W. Gray, H.-W. Spiess and V. Vill (Weinheim: Wiley-VCH), pp. 801–833; (*b*) Date, R. W., Imrie, C. T., Luckhurst, G. R., and Seddon, J. M., 1992, *Liq Cryst.*, **12,** 203.
[17] (*a*) Watanabe, J., Komura, H., and Niori, T., 1993, *Liq Cryst.*, **13,** 455; (*b*) Niori, T., Adachi, S., and Watanabe, J., 1993, *Liq Cryst.*, **19,** 139.
[18] Watanabe, J., Izumi, T., Niori, T., Zennyoji, M., Takanishi, Y., and Takezoe, H., 2000, *Mol. Cryst. liq Cryst.*, **346,** 77.
[19] (*a*) Suzuki, Y., Isozaki, T., Kusumoto, T., and Hiyama, T., 1995, *Chem. Lett.*, 719; (*b*) Suzuki, Y., Isozali, T., Hashimoto. S., Kusumoto, T., Hiyama, T., Takanishi, Y., Takezoe, H., and Fukuda, A., 1998, *J. mater. Chem.*, **6,** 753.
[20] Itoh, K., Kabe, M., Miyachi, K., Takanishi, Y., Ishikawa, K., Takezoe, H., and Fukuda, A., 1997, *J. mater. Chem.*, **7,** 407.
[21] (*a*) Goodby, J. W., Waugh, M. A., Stein, S. M., Chin, E., Pindak, R., and Patel, J. S., 1989, *J. Am. chem. Soc.*, **111,** 8119; (*b*) Goodby, J. W., Petrenko, A., Hird, M., Lewis, R. A., Meier, J., and Jones, J. C., 2000, *Chem. Commun.*, 1149.
[22] (*a*) Gray, G. W., 1986, *Zehn Arbeiten uber Hüssige Kristalle, Kongress-und Tagung-berichte der Martin-Luther-Universität, Halle-Wittenberg*, pp. 22–42; (*b*) Kutsumizu, S., Yamaguchi, T., Kato, R., and Yano, S., 1999, *Liq Cryst.*, **26,** 567.
[23] Goodby, J. W., Dunmur, D. A., and Collings, P. J., 1995, *Liq Cryst.*, **19,** 703.